

# Supplementary Material for Unsupervised Adaptation Learning for Hyperspectral Imagery Super-resolution

Lei Zhang<sup>1,2\*</sup>, Jiangtao Nie<sup>2\*</sup>, Wei Wei<sup>2</sup>, Yanning Zhang<sup>2</sup>, Shengcai Liao<sup>1</sup> and Ling Shao<sup>1</sup>

<sup>1</sup>Inception Institute of Artificial Intelligence (IIAI), United Arab Emirates

<sup>2</sup>School of Computer Science, Northwestern Polytechnical University, China

In this material, we provide some other experimental results of the proposed method to further clarify its effectiveness in fusion based hyperspectral image (HSI) super-resolution (SR).

## 1. Effect in degeneration estimation

As Section 4.3 of the main manuscript, we test the proposed method under various unknown degenerations on the CAVE dataset with SR scale  $s = 8$ . Here we mainly focus on demonstrating the effectiveness of the proposed in degeneration estimation, *i.e.*, estimating the kernel  $\mathbf{k}$  in the unknown degeneration  $\mathbf{H}$ .

**Estimation for different kernels** We utilize four kernels shown in Figure 1 and a fixed level (*e.g.*, 40db) of noise corruption to produce different degenerations  $\mathbf{H}$ . For each  $\mathbf{H}$ , we generate the corresponding observed images, *e.g.*  $\mathbf{X}$  and  $\mathbf{Y}$ , as mentioned in the manuscript and then feed them into the proposed method for degeneration estimation. The estimated kernels are shown in Figure 1. For convenient comparison, we crop the estimation results with the same size as the ground truth. As can be seen, the proposed method can produce good estimate for all four kernels.

**Estimation under different noise levels** In this section, we fix  $\mathbf{k}_1$  as the kernel and introduce three different levels (*e.g.* 30db, 35db, 40db) of noise corruption to produce the degeneration  $\mathbf{H}$ . Similar to the above experiment, we employ the proposed method to estimate the kernels in the unknown  $\mathbf{H}$ . The estimation results are sketched in Figure 2. It can be seen that the proposed method can accurately estimate the kernels under various levels of noise corruption.

## 2. Effect of training samples number

In the proposed method, we require a few training samples to pretrain the fusion module with synthetic degenera-

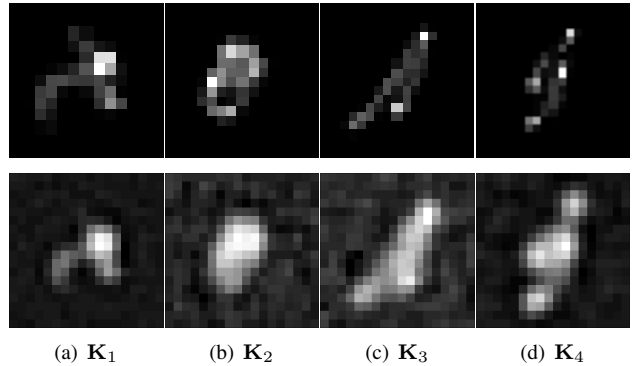


Figure 1. Four different kernels utilized to produce the degeneration  $\mathbf{H}$  in test as well as the estimation results by the proposed method on the CAVE dataset with scale  $s = 8$ . From left to right, they are  $\mathbf{K}_1$ ,  $\mathbf{K}_2$ ,  $\mathbf{K}_3$  and  $\mathbf{K}_4$ . The ground truth and the estimation of these kernels are shown at the first and the second rows, respectively.

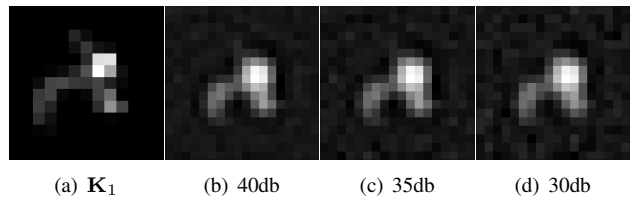


Figure 2. The estimated results of  $\mathbf{K}_1$  under three different levels (*e.g.*, 40db, 35db and 30db) of noise corruption on the CAVE dataset with scale  $s = 8$ .

tions. To demonstrate the effect of training samples number on the performance of the proposed method, we conduct experiments using different number of training samples on the CAVE dataset. Without loss of generality, we produce the test degeneration with the kernel  $\mathbf{k}_1$  in Figure 1 and 40db Gaussian white noise. The SR scale is fixed as 8. The numerical results are reported in Table 1. As can be seen, as the training sample number decrease, the performance slightly drops. However, even when there is only 1 train-

\*The first two authors contributed equally to this work. The corresponding author is Wei Wei (email: weiweinwpu@nwpu.edu.cn).

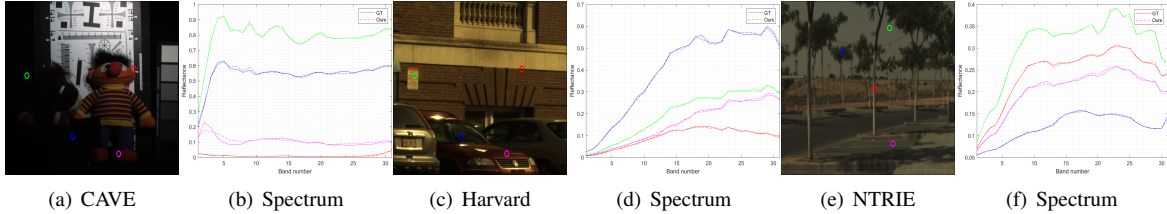


Figure 3. The spectrum estimated by the proposed method on three benchmark HSI datasets. ('GT' and 'Ours' in the figure denote the result obtained from the ground truth and the proposed method)

Table 1. Effect of training sample number (TSN) on the performance of the proposed method.

	RMSE	PSNR	SAM	SSIM
TSN=1	3.61	37.73	7.06	0.9694
TSN=6	2.22	41.87	6.84	0.9849
TSN=12	<b>1.85</b>	<b>43.23</b>	<b>6.72</b>	<b>0.9862</b>

ing sample, the proposed method still outperforms most of competitors mentioned in Table 4 of the main manuscript. This is because of the the adaptation module that can refine the image-specific details via unsupervised learning even with a rough estimation output by the pre-trained fusion module.

### 3. Performance in spectral reconstruction

In this section, we test the proposed method on three benchmark datasets, (*e.g.*, CAVE, Harvard and NTRIE) with the degeneration that  $\mathbf{H}$  is produced by kernel  $\mathbf{k}_1$  under 40db of noise corruption and the scale  $s=8$ . To illustrate the effectiveness of the proposed in reconstructing the spectra in super-resolution, we separately select one per dataset and then sketch the reconstructed spectrum at four different positions in the image, as shown in Figure 3. Clearly, the recovered spectra are very close to the ground truth.

### 4. Reconstruction procedure

In this section, we plot the reconstruction performance curves versus the unsupervised learning epochs. Specifically, we select the 'chart\_and\_stuffed\_toy' image from the CAVE dataset as the testing data and evaluate the proposed method when the SR scale  $s$  is 8 and the degeneration is produced by  $\mathbf{k}_1$  and 40db noise. The obtained RMSE, PSNR, SAM and SSIM values with respect to the unsupervised learning epochs are depicted in Figure 4. As can be seen, the SR performance increases as the optimization epochs of unsupervised learning proceeds. More importantly, the performance increases faster at the beginning, then slows down and ultimately converges. Thus, we can make a trade-off between performance and efficiency by reducing

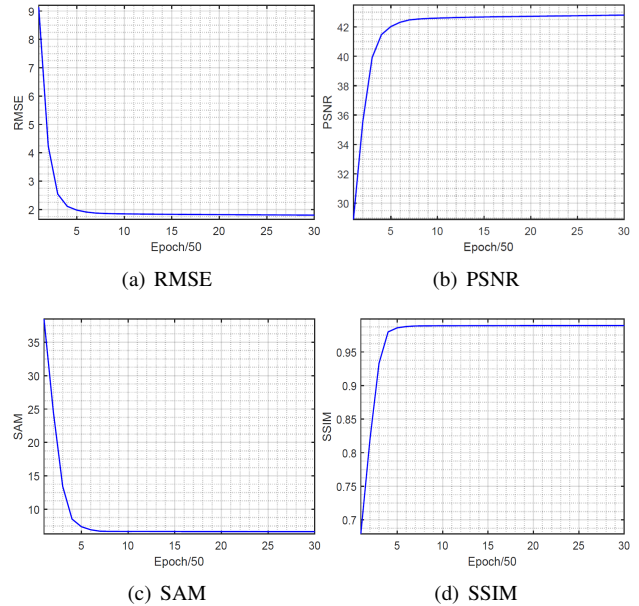


Figure 4. The performance curves versus the unsupervised learning epochs.

the number of optimization epochs.